Atmos. Chem. Phys. Discuss., 10, 7641–7674, 2010
www.atmos-chem-phys-discuss.net/10/7641/2010/

Atmospheric Chemistry and Physics Discussions

This discussion paper is/has been under review for the journal Atmospheric Chemistry and Physics (ACP). Please refer to the corresponding final paper in ACP if available.

Estimation of Antarctic ozone loss from Ground-based total column measurements

J. Kuttippurath[1], F. Goutail[1], J.-P. Pommereau[1], F. Lefèvre[2], H. K. Roscoe[3], A. Pazmiño[1], W. Feng[4], and M. P. Chipperfield[4]

[1]Université Versailles-Saint-Quentin, CNRS/INSU, UMR 8190 LATMOS-IPSL, 91371 Verrières Le Buisson, France
[2]UPMC Univ. Paris 06, CNRS/INSU, LATMOS-IPSL, 75005 Paris, France
[3]British Antarctic Survey, Cambridge, UK
[4]School of Earth and Environment, University of Leeds, UK

Received: 5 February 2010 – Accepted: 12 March 2010 – Published: 24 March 2010

Correspondence to: J. Kuttippurath (jayan@aero.jussieu.fr)

Published by Copernicus Publications on behalf of the European Geosciences Union.

Abstract

The passive ozone method is used to estimate ozone loss from ground-based measurements in the Antarctic. A sensitivity study shows that the O_3 loss can be estimated within an accuracy of ~4%. The method is then applied to the observations from Amundsen-Scott/South Pole, Arrival Heights, Belgrano, Concordia, Dumont d'Urville, Faraday, Halley, Marambio, Neumayer, Rothera, Syowa and Zhongshan for the diagnosis of ozone loss in the Antarctic. On average, the five-day running mean of the vortex averaged ozone column loss deduced from the ground-based stations shows about 53% in 2009, 59% in 2008, 55% in 2007, 56% in 2006 and 61% in 2005. The observed O_3 loss and loss rates are in very good agreement with the satellite observations (Ozone Monitoring Instrument and Sciamachy) and are well reproduced by the model (Reprobus and SLIMCAT) calculations.

The historical ground-based total ozone measurements show that the depletion started in the late 1970s, reached a maximum in the early 1990s, stabilising afterwards at this level until present, with the exception of 2002, the year of an early vortex break-up. There is no indication of significant recovery yet.

At southern mid-latitudes, a total ozone reduction of 40–50% is observed at the newly installed station Rio Gallegos and 25–35% at Kerguelen in October–November of 2008–2009 and 2005–2009 (except 2008) respectively, and of 10–20% at Macquarie Island in July–August of 2006–2009. This illustrates the significance of measurements at the edges of Antarctica.

1 Introduction

Discovered in 1985 from Dobson ground-based (GB) measurements at Halley Bay (now Halley) (Farman et al., 1985), ozone loss has been continuously monitored since then by a series of satellites, by ground-based instruments and by ozonesondes at various stations in the framework of the international WMO–GAW (World Meteorological

ACPD

10, 7641–7674, 2010

Organisation–Global Atmospheric Watch) programme (WMO, 1993) and the Network for Detection of Atmospheric Composition Change (NDACC). The satellites have the advantage of global coverage, but because they cannot observe at Solar Zenith Angle (SZA) >84° and thus not during the deep winter months, the maintenance of an independent ground-based capacity is absolutely essential. There are other reasons for that: i) the limited life-time of space-borne sensors which cannot always be immediately replaced, ii) the possible progressive degradation of their measurements, iii) the discontinuity of the measurements between systems employing different instruments and retrieval algorithms. In contrast, though of limited geographical coverage, ground-based stations present the unique advantage of continuous record, easy repair or replacement if necessary. Those measuring at visible wavelengths, such as SAOZ (Système d'Analyse par Observation Zénithale) spectrometers used in the following study, are capable of making reliable measurements until 91° SZA, which is throughout winter at the polar circle.

Based on similar approach, such a measurement cluster was used in the Arctic for calculating daily ozone loss rate, that is separating the contribution due to transport and photochemical depletion in the total ozone evolution during the winter (Goutail et al., 1999, 2005). The method, called Passive or Tracer Method makes use of Chemical Transport Model (CTM) simulations forced by meteorological analyses in which photochemistry is deactivated, for subtracting the contribution of transport from the ozone change during the winter.

The objective of the present study is to apply the same method in the Antarctic for the yearly evaluation of ozone loss. The measurements available are those of three SAOZ instruments in the Antarctic deployed since 1988 in Dumont d'Urville for the oldest (Fig. 1) and Concordia in 2007 for the latest. In addition, measurements from a DOAS (Differential optical absorption spectroscopy) instrument, six Dobson including the historical stations Halley, South Pole, Faraday and Syowa, and two Brewer spectrophotometers are used. Further, to find the spread of the ozone hole, analyses for selected mid-latitude stations are performed. Table 1 and Fig. 2 show details of the

stations. The CTM simulations used are the Reprobus model of the CNRS and the SLIMCAT model of the University of Leeds. The ground-based ozone loss estimations are compared to space-borne observations from OMI (Ozone Monitoring Instrument) on-board AURA and SCIAMACHY (SCIA) on Envisat.

2 Ozone column measurements

2.1 SAOZ

The zenith sky SAOZ UV-vis spectrometers (Pommereau and Goutail, 1988) operate at 300–650 nm, looking at sunlight scattered from the zenith sky during twilight. Ozone is measured in the Chappuis band (450–650 nm) at high SZA between 86 and 91° in every morning and evening, allowing continuous monitoring throughout the year at the polar circle. As concluded from various inter-comparison exercises (Roscoe et al., 1999; Vaughan et al., 1997), the measurements of different SAOZ instruments are consistent within ±3%. The main source of uncertainty in those measurements is the air mass factor (AMF) and the difference in AMF between inside and outside the ozone hole can be up to 10%.

2.2 DOAS

This is a similar instrument to SAOZ but with differences of detail, e.g. light is collected by a small telescope and fed to the spectrograph using two depolarising quartz fibre bundles. The spectrograph consists of a UV and a visible channel. The ozone measurements are performed (at 84–90° SZA) in visible range, 490–555 nm, similar to SAOZ. Ozone slant column densities are converted using AMF's estimated from AMFTRAN Monte Carlo Radiative Transfer Model. The accuracy of ozone vertical column density retrieved from the Neumayer DOAS is about 2% and is described in detail by Frieß et al. (2005).

2.3 The Dobson spectrophotometer

The instrument consists of a double prism monochromator to measure the differential absorption of ozone in UV spectra (Dobson, 1957). Individual measurements are performed by looking at the direct sun by clear sky and are averaged to a daily mean. Nevertheless, those measurements are limited to SZA <80° i.e. after mid-August at the polar circle. As the instrument requires calibration, comparison with the well-calibrated Dobson #83 (Boulder, USA) is carried out. However, at South Pole calibration with this instrument may not be that accurate (because of high latitude and large SZA measurements) and hence, it may slightly affect its accuracy. The estimated relative error in individual direct sun total ozone measurements by the instrument is 0.5% or 1 DU (Basher, 1982).

2.4 The Brewer spectrophotometer

Brewer measurements also make use of differential absorption in the UV region (Brewer, 1973). The determination of total ozone is similar to that of the Dobson. Sensitivity of the instrument is better than that of the Dobson. As in the case of the Dobson, an empirical relation between simultaneous direct sun and zenith sky has to be established if zenith observations are to be taken. Calibration of the instrument is essential. A well calibrated Brewer direct sun measurement has an error comparable to that of the Dobson.

2.5 OMI on AURA

The OMI sensor on the AURA satellite began to operate in 2004 as a successor to the Total Ozone Mapping Spectrometer (TOMS) (Levelt et al., 2006). The nadir viewing UV-visible spectrometer measures solar light scattered by the atmosphere with a spatial resolution at nadir of 13×24 km. The sun-synchronous orbit of AURA and the wide viewing angle of OMI enable daily global coverage of the sunlit portion of the Earth.

The data presented are retrieved using the TOMS v8 algorithm. The retrieval makes use of two wavelengths: 331.2 and 360 nm for high ozone and high solar zenith angle, while 317.5 and 331.2 nm are used for most conditions. The uncertainty of the product is estimated to be 2–5% (Bhartia and Wellemeyer, 2002), but limited to SZA <84°.

2.6 SCIAMACHY on Envisat

SCIAMACHY (Scanning Imaging Absorption Spectrometer for Atmospheric CHartography), an imaging spectrometer on board Envisat launched into orbit in 2002, utilises nadir, limb and sun/moon occultations for ozone column retrievals (Bovensman et al., 1999). The data are recorded from the transmitted, back scattered and reflected solar radiation from the atmosphere at 240–1700 nm. The instantaneous field of view spans 2.6 km in the vertical and 110 km in the horizontal direction at the tangent point. We use total column retrieved with the v2 algorithm based on TOSOMI (Total Ozone retrieval scheme for SCIAMACHY based on the OMI DOAS algorithm). The estimated accuracy of the ozone column is about 2–3.3% (Eskes et al., 2005).

3 Estimation of ozone loss

To find chemical ozone depletion from measurements, tracer calculation by a CTM is required. Simulations from Reprobus for 2006–2009 and SLIMCAT for 2005 are used, as the data from the former was not available in 2005. Nevertheless, a detailed discussion on the model calculations is beyond the scope of this study as it focuses on the method and measurements. The details of tracer calculations in the models are introduced in the following sections and the analysis method is described afterwards.

3.1 REPROBUS

The Reprobus CTM has been widely used in previous studies of stratospheric chemistry (Lefèvre et al., 1994, 1998). The model uses a hybrid σ-pressure vertical coordi-

ACPD
10, 7641–7674, 2010

nate for which winds and temperatures are driven by the 3-hourly ECMWF operational system on 60 vertical levels to 0.1 hPa until February 2006, then 91 levels to 0.01 hPa. Vertical advection is computed directly from the analysed winds. The simulations presented here were integrated on a global grid with a horizontal resolution of 2°×2°. Chemical species are transported by a semi-Lagrangian code (Williamson and Rasch, 1989). The model includes a comprehensive description of stratospheric chemistry. Absorption cross-sections and kinetics data are based on Sander et al. (2006), except the absorption cross sections of Cl_2O_2 were taken from Burkholder et al. (1990) and are extrapolated to 450 nm. Monthly varying H_2SO_4 fields leading to the formation of liquid aerosols in the CTM are computed from the outputs of a 2-D-model long-term simulation, which takes into account impacts of volcanic eruptions (Bekki et al., 1996). The heterogeneous chemistry module includes reactions on binary and ternary liquid aerosols as well as on water-ice particles. The composition of liquid aerosols is calculated analytically (Luo et al., 1995). The ice particles are assumed to incorporate HNO_3 in the form of nitric acid trihydrate (NAT) (Davies et al., 2002). Cl_y and Br_y are explicitly calculated from their long-lived sources at the surface (WMO, 2007) and are therefore time dependent. An additional 6 pptv of bromine in the form of CH_2Br_2 is added to Br_y to represent the contribution of brominated short lived species reaching the stratosphere.

3.2 SLIMCAT

SLIMCAT is an off-line 3-D CTM described in detail by Chipperfield (1999). The model uses hybrid σ-θ as the vertical coordinate and extends from the surface to a top level which depends on the domain of the forcing analyses (Feng et al., 2007a,b). Here the horizontal winds and temperatures are specified using ECMWF operational data of 60 vertical levels to 0.1 hPa. Vertical advection in the θ-level domain (above 350 K) is calculated from diabatic heating rates using the National Centre for Atmospheric Research Community Climate Model radiation scheme (Feng et al., 2005; Chipperfield, 2006). Chemical tracers are advected by conservation of second-order moments

(Prather, 1986). The model describes the main stratospheric chemical species O_x, HO_x, NO_y, Cl_y, Br_y as well as source gases and a treatment for CH_4 oxidation. It contains a detailed gas-phase stratospheric chemistry scheme. As in Reprobus, the photochemical data are based on Sander et al. (2006) and the absorption cross sections of Cl_2O_2 are taken from Burkholder et al. (1990) extrapolated to 450 nm. The model treats heterogeneous reactions on liquid aerosols, NAT and ice (Chipperfield, 1999) and denitrification schemes (Davies et al., 2002). An extra 6 pptv of bromine reaching the stratosphere from short-lived species is also included in the calculations (Feng et al., 2007b).

3.3 The passive tracer method

The ozone loss by the passive method (Goutail et al., 1999, 2005) is computed by subtracting passive ozone (ozone simulated without interactive chemistry) from measured ozone. Large changes in total ozone inside the vortex are related to convergence or divergence changes in tropopause height, planetary wave induced adiabatic motions and diabatic descent due to radiative cooling. To evaluate the loss inside the vortex, the Nash et al. (1996) criterion is used to find the vortex edge (the first derivative of potential vorticity (PV)). A sensitivity test was conducted using criterion of 35 PV unit (pvu) and 45 pvu (1 pvu is 10^{-6} Km^2 kg^{-1} s^{-1}). While the low PV criterion adds noise, the high PV criterion makes the data sparse. As expected, though there were differences in number of observations inside the vortex when using different criteria, the final results were similar. So Nash et al. (1996) appears to be the optimum criterion for the loss estimation. Some apparent noise in the vortex limit data is exempted from manual inspection. The PV data used to differentiate the vortex measurements were generated from the MIMOSA advection model (Hauchecorne et al., 2002) forced by the ECMWF meteorological analyses.

The vortex edge calculated at 475 K, where the concentration of ozone has its maximum in spring, is selected for the ozone loss estimation. The period of assessment starts in July and extends until November.

Figure 3 explains the basics of the tracer scheme with relevant data at Dumont d'Urville for the Antarctic winter 2007. The day to day variations due to vortex positions are well captured by the measurements and simulations. From July onwards, the ozone values in the vortex decrease with time while they increase outside. The ozone columns, both measured and calculated, are anti-correlated with the PV values: high PV corresponds to low ozone inside the vortex. The SAOZ observations are continuous throughout the winter, while OMI/SCIA starts in mid-August, missing thus the onset of the ozone loss process, but both observations are very consistent afterwards.

The chemical ozone loss is then estimated by finding the difference between the passive ozone computed by the CTM and the ozone measured from the ground or space. This procedure is repeated for each station and then sorted for inside the vortex. The example of year 2007 is given in Fig. 4. The loss starts at Rothera at the edge of the vortex in mid-July, when the vortex is displaced to the sunlit parts. So the stations at the edge of the vortex, such as Dumont d'Urville and Rothera, are subjected to ozone loss early in the winter. As the day gets longer and the light penetrates deeper inside, the stations Concordia and Arrival Heights followed by Neumayer, Halley, Syowa, Belgrano and Amundsen-Scott undergo the ozone depletion. Measurements at the latter stations were possible only in late August or September because of the lack of sunlight to carry out observations. The figure clearly shows the late winter start of ozone loss in the deep vortex at these high latitude stations, Concordia in particular (South Pole measurements start even later, by mid-September). This delayed start also produces a step like feature in the mean ozone loss curves in July-mid August period.

As in the case of the time of onset, the intensity of ozone loss is also related to position of the stations. The sites well-inside the vortex experience more loss than those at the edge. Therefore, South Pole, Belgrano or Neumayer observe more severe loss than Dumont d'Urville or Faraday in each winter. The loss at Concordia and Rothera is less than that of South Pole and larger than those of Dumont d'Urville due to the strength and longevity of the vortex over the respective locations.

The results feature three distinct phases of the Antarctic ozone loss as marked in

Fig. 4. The first stage of the process starts in July and ends in late September, where rapid loss of ozone occurs with the return of the sun over the peninsula. The ozone loss rate is largest in this period. The starting time of this phase varies from May to July depending on the temperature, the time of vortex formation and its location. If the temperature is very low and the vortex appears in early winter and the axis of the vortex is shifted in latitude, there might be some ozone loss in May-June, hence this active stage may start in May itself. The cumulative maximum of the depleted ozone is generally observed in early October, afterwards the loss stops when PSCs (Polar Stratospheric Clouds) are no longer forming because of higher temperatures. The depth of the ozone hole reduces then more or less slowly depending on vortex erosion, exchange with mid-latitudes, and location of the station. Therefore, the edge region stations, i.e., Dumont d'Urville, Marambio and Rothera, recover more rapidly. The ozone hole is not homogeneous. Depending on the location of the station relative to the vortex, the loss can vary within ±10% (20 DU). The ozone hole then disappears by the end of November or early December as in 2006, except the unprecedented split in 2002. It is during this period that vortex pieces or filaments more or less filled-in could be observed at lower latitudes as in Kerguelen at 49° S.

3.3.1 Error analysis

In order to estimate the uncertainty in the loss analysis, we diagnosed the ozone loss under various conditions for a given station. Figure 5 shows the ozone loss estimated with SAOZ, OMI and SCIA using Reprobus and SLIMCAT (both with T42 and T21 resolution) for Dumont d'Urville in 2007. The stations at the edge region show more spread than those inside the vortex (Dumont d'Urville shows the largest). We use the SAOZ/ground-based ozone loss analysis with Reprobus tracer using Mimosa PV and Nash vortex edge as the control, since the simulated results match well with measurements. To find the uncertainty of the method, the difference between the control and the ozone loss was estimated with other setups, as shown in the figure. The root sum square (RSS) of all these differences as well as the uncertainties of the observations

yield a deviation up to 4.4% (0–21 DU) depending on day.

The RSS computation includes all the prime processes that affect the accuracy of the method. Those are: the systematic differences between the instruments, drop in measured ozone due to presence of PSCs, difference in AMF profile shapes (considered by the measurement uncertainties of respective instruments), differences in simulated profiles with measurements when ozone varies rapidly (counted by using tracers from different models of varying horizontal and vertical resolution), shifts in location of estimated vortex edge (by testing with different vortex criteria, different PV data sets and horizontal resolution of the model). Since size of the vortex can be smaller above the analysis level of 475 K, air outside the vortex cannot be ruled out and was not possible to account by these experiments.

3.4 Conclusions on the method

There are a few parameters that influence the strength of the analysis. The most evident are the realism of the tracer field in the models and the vortex edge calculation from potential vorticity. We tested how the derived ozone loss varies with the expected changes in these parameters. These tests were repeated for the overpass measurements from satellite observations as well. The RSS of the deviations including measurement accuracies is within 4%. Since the accuracy of the measurements is of the order of 3–5% and the total error from RSS is ~4%, the small contribution from other input shows the consistency and potency of the method. In addition, the use of different model setups ensures that the estimation provides consistent results and affirms that the method is sound. The main dispersion of loss evaluations comes from the inhomogeneous distribution of ozone in the vortex, of ±2–10% at the beginning when only edge stations are exposed to sunlight, reducing to ±0–5% at the end when depletion has stopped.

4 Application of the method to the recent Antarctic winters 2005–2009

We now examine the variability of the Antarctic ozone loss between 2005 and 2009. The analyses with SCIA exclude the South Pole because of the unavailability of measurements.

Figure 6 shows the ozone loss derived from ground-based, OMI, SCIA and the CTMs (Reprobus for the winters 2006–2009 and SLIMCAT in 2005) for the recent winters and we begin with the discussion of the most recent year. The ozone depletion started by the first week of July in 2009 and peaked to 53% by late September. The satellite observations, both OMI and SCIA, agree well with the ground-based analysis, except for OMI in October. The offset in OMI observations could be due to the anomaly detected in the data. The ozone loss rate calculated between day 225 and 275 (the same time window is used in all years) shows 0.62 for ground-based, 0.58 for OMI, 0.54 for SCIA and 0.55%/day for the model. Further details of these analyses are listed in Table 2.

In 2008, the ozone depletion started in early July and the loss from ground-based measurements shows its peak by early October, about 59%. Similar results are found from the loss computed with satellite measurements and model calculations, where the differences are within ±2%. The loss rates analysed from the measurements and model exhibit similar values, about 0.8%/day, but slightly less from SCIA.

In 2007, as found for other winters, the ozone loss started in July and reached its peak by mid-October. The loss derived from ground-based and OMI observations exhibit similar maxima of 55%, while 3% more and less in the loss estimated with Reprobus chemical code and SCIA measurements, respectively. The ozone loss rate analysed from different data sets are 0.62 for ground-based, 0.54 for OMI, 0.47 for SCIA and 0.66%/day for Reprobus.

In 2006, the maximum loss from ground-based observations is 56%, consistent with that of OMI measurements. The loss found from SCIA and Reprobus data show slightly lower values, of about 53%. The estimated loss in July–September from the model is slightly smaller than that of ground-based, even if both return similar loss rates of

0.71%/day.

In 2005, large loss was observed in early winter. A maximum depletion of 61% is found from the ground-based analysis, whereas 1% more in SLIMCAT calculations. The loss analysed from satellite observations find agreeable results within 2%. The observed loss rate are 0.53, 0.50, 0.50 and 0.75%/day for ground-based, OMI, SCIA and SLIMCAT respectively.

5 Total ozone inter-annual variations and trends

5.1 Inter-annual variation of ozone loss in the Antarctic

The inter-annual variation in ozone loss is not large in the Antarctic because of its saturation. The general behaviour of the ozone loss with time and chemistry involved is alike in all winters, but the cumulative loss, period of maximum depletion and longevity of the ozone hole alter in accordance with the strength of the vortex. Its evaluation from ground and space is very consistent, showing insignificant differences, around 55%. The first signs of depletion are observed during the first week of August in 2007, 2008 and 2009, one week earlier in 2006 and 3 weeks earlier in 2005. The depletion stops during the last week of September, except in 2006 when it extended until the first week of October. In all years the ozone hole could be followed until the 3rd and 4th week of November.

Figure 7 illustrates the daily minimum temperature from ECMWF within 50–90° S at 475 K for 2005–2009. In general, temperatures below the formation of nitric acid trihydrate (T_{NAT}) are found from mid-May until October. Temperatures below the freezing point of water-ice (T_{ICE}) occur from June to late September. Among the last four winters, 2007 shows the lowest temperatures in May–June, 2008 shows the lowest in mid-July to mid-August and 2006 shows the lowest in mid-September to November. The recent winter 2009 was generally colder than 2008 and 2005 and the winter 2007 shows the warmest September–November and earliest vortex dissipation. The winter

2006 was one of the coldest, in which the breakdown of the vortex was in December.

As expected from their similar temperatures, the cold winters 2006, 2008 and 2009 show little difference in ozone loss. The maximum ozone loss was found early in 2006 as compared to other winters because of the colder temperatures and well formed early vortex, whereas the warm winter 2007 measures relatively lower loss. The satellite measurements find similar values of ozone depletion in each winter, where the differences with ground-based observations are within 3%.

5.2 Total ozone at southern high latitudes

Ozone loss estimation from measurements greatly depends on tracer simulation from the models. So we now examine the inter-annual variation of ozone measurements at the stations. Since measurements are available for decades, this diagnosis does not restrict to 2005–2009, as in the previous ozone loss estimation. However, a rigorous statistical analysis is beyond the scope of this work and will not be attempted. Figure 8 displays the October mean of total ozone and stratospheric chlorine together with EESC (Equivalent Effective Stratospheric Chlorine) in the Antarctic. The four historic stations Halley, Syowa, South Pole and Faraday have measurements since the 1950s. These show large increase in ozone loss until early 1990s, but the control of emissions by various treaties helped the situation to improve and hence, saturation of the ozone loss is evident after 1993 at all stations in conjunction with decrease in ozone depleting substances as indicated by EESC.

Figure 9 zooms the ozone variability in 1994–2007 from all Antarctic stations. As expected, the stations well inside the continent, South Pole, Belgrano and Halley, register lower values (150–200 DU) than those of Dumont d'Urville, Faraday and Rothera (250–350 DU). However, the measurements indicate neither increasing nor decreasing trend, corroborating the saturation of ozone loss in the Antarctic, consistent with the ozone loss estimations.

5.3 Total ozone in the southern mid-latitudes

The ozone loss analysis for the Antarctic will not be completed without assessing its impact on mid-latitudes. Therefore, we now examine the ozone loss computed above three stations located at three different regions in southern mid-latitudes, well outside the Antarctic continent. This is particularly important since very low ozone around 250 DU are observed on some days at these stations during recent winters. Figure 10 shows the ozone loss estimated with Reprobus tracer using Rio Gallegos, Kerguelen and Macquarie Island measurements in 2005–2009. Extension of the vortex or spread of filaments to the mid-latitudes is absent in some years, as in 2005 at Macquarie Island and 2008 at Kerguelen. Further, there were no vortex events found over Lauder for 2005–2009.

The ozone loss analyses expose the vortex a few days in October 2008 and November 2009 and estimate a maximum loss of 40–45% (150–200 DU) at Rio Gallegos. A similar scale (30-50%) of loss from relatively higher number of vortex occurrences is also estimated at Ushuaia using the SLIMCAT tracer in September-November 2004–2008 (not shown). Except in 2008, about 30% (50–100 DU) of ozone is lost at Kerguelen when the vortex passed over the station in October–November of each year. In contrast, passage of the vortex over Macquarie Island was found mostly during early winter and thus, the ozone loss is relatively smaller (10–20% or up to 100 DU). However, this is equal to that of the Antarctic during the same period.

In order to diagnose the inter-annual variations, the October mean of total ozone from selected mid-latitude stations are examined in Fig. 11. As found for high latitude stations, there is a weak signal of loss in 1975–1993 (about 50 DU) at Lauder and Macquarie Island in tune with the increase of EESC. The measurements at cities far outside the Antarctic, Perth, Buenos Aires and Melbourne, leave no clear trend since the 1960s. On the other hand, the stations Ushuaia, Comodoro Rivadavia and Kerguelen influenced by vortex filaments/displacements show large inter annual variability. Nevertheless, the trend in October ozone is similar to that of Antarctic stations.

6 Conclusions

The passive method is shown to provide ozone loss estimation within an accuracy of about 4%. The scheme was then applied to find the ozone depletion during recent Antarctic winters. The ground-based measurements from Amundsen-Scott, Arrival heights, Belgrano, Dumont d'Urville, Concordia, Faraday, Halley, Marambio, Neumayer, Rothera, Syowa and Zhongshan show substantial loss in 2005–2009. The depletion is shown to start at the edge of the vortex by July in every winter and each station shows different timings for the starting of ozone loss in accordance with exposure to sunlight. Further, the magnitude of loss is also different at each site in line with the temperature, PV, PSCs, and prevailing heterogeneous chemistry.

The biggest advantage of the ground-based visible instruments (e.g. SAOZ) is the capability of measuring early winter ozone loss and thus covering the whole winter/spring to enable the complete evaluation, whereas the satellite measurements start in spring only. The OMI and SCIA observations exhibit remarkably good agreement with the ground-based measurements at each stations, their mean ozone loss and inter-annual variations. Even if the South Pole measurements were not available with SCIA, the estimated ozone loss and loss rates for each winter agree well with that of ground-based observations. The models imitate the ozone loss features and loss rates very well and reproduce the maximum loss within ±5% difference.

The year-to-year differences in ozone loss are not large in the Antarctic, which is estimated around 55% on average since 2005. The historical ground-based stations total column measurements do show that the depletion started in the late 1970s, with a maximum in the early 1990s, stabilising afterwards at this level until present, with the exception of 2002, the year of an early vortex break-up. There is no sign of convincing recovery yet.

Another important feature is the effect of the ozone hole at mid-latitudes. The SAOZ measurements at Kerguelen and Rio Gallegos, the first observations from the latter, reveal severe ozone loss (10–45% or 50–200 DU) even in moderately cold winters,

which reiterates the value of observations at mid-latitudes.

Acknowledgements. We thank Udo Frieß of Institute for Environmental Physics of the University of Heidelberg, Germany for the Neumayer data, Jonathan Shanklin of British Antarctic Survey for the BAS Antarctic stations data, Eric Nash of NASA GSFC, Greenbelt MD for the vortex edge data, Cathy Boonne of Centre for Atmospheric Chemistry Products and Services (Ether) for providing with MIMOSA potential vorticity and Reprobus chemistry data, and Eduardo Quel, Elian Wolfram and Jacobo Salvador of CEILAP (CITEFA-CONICET) for the Rio Gallegos data.

The total stratospheric chlorine data was taken from European Environment Agency website (http://dataservice.eea.eu.int/dataservice) and EESC data for the Antarctic and mid-latitudes were obtained from National Oceanic and Atmospheric Administration website (http://www.esrl.noaa.gov/gmd/odgi/).

The data used in this publication were obtained as part of the Network for the Detection of Atmospheric Composition Change (NDACC) and are publicly available (see http://www.ndacc.org). The French stations are supported by IPEV (Institut Paul Emile Victor), INSU (Institut des Sciences de l'Univers) and CNES (Centre National d'Etudes Spatiales).

A good part of the data used in this work is also taken from World Ozone and Ultraviolet Radiation Data Centre (WOUDC) and are publicly available (see http://www.woudc.org). We take this opportunity to thank the respective national governing bodies and research establishments, who maintain the stations.

We thank the station scientists and instrument operators at all ground-based stations. We also thank Sophie Godin-Beekmann (CNRS/INSU, Paris) for her help and support during this project.

The work is supported by a funding from French ANR/ORACLE and EC/SCOUT-O_3 projects.

The publication of this article is financed by CNRS-INSU.

References

Basher, R. E.: Review of the Dobson spectrophotometer and its accuracy, WMO Global Ozone Research and Monitoring Project, Report No. 13, WMO, Geneva, 1982. 7645

Bekki, S., Pyle, J. A., Zhong, W., Toumi, R., Haigh, J. D., and Pyle, D. M.: The role of microphysical and chemical processes in prolonging the climate forcing of the Toba eruption, Geophys. Res. Lett., 23, 2669–2672, 1996. 7647

Bhartia, P. K. and Wellemeyer, C. W.: TOMS-V8 total O_3 algorithm, NASA Goddard Space Flight Centre, Greenbelt, MD, OMI Algorithm Theoretical Basis Document Vol II., 2387 pp., 2002. 7646

Brewer, A. W.: A replacement for the dobson spectrophotometer?, Pure Appl. Geophys., 919, 1136, 106–108, 1973. 7645

Bovensman, H., Burrows, J. P., Buchwitz, M., Frerick, J., Noël, S., Rozanov, V. V., Chance, K. V., and Goede, A. P. H.: SCIAMACHY: mission objectives and measurement modes, J. Atmos. Sci. 56, 127–150, 1999. 7646

Burkholder, J. B., Orlando, J. J., and Howard, C. J.: Ultraviolet absorption cross-sections of Cl_2O_2 between 210 and 410 nm, J. Phys. Chem., 94, 687–695, 1990. 7647, 7648

Chipperfield, M. P.: Multiannual simulations with a Three-Dimensional chemical transport model, J. Geophys. Res., 104, 1781–1805, 1999. 7647, 7648

Chipperfield, M. P.: New version of the TOMCAT/SLIMCAT off-line chemical transport model: Intercomparison of stratospheric tracer experiments, Q. J. Roy. Meteorol. Soc., 132, 1179–1203, doi:10.1256/qj.05.51, 2006. 7647

Davies, S., Chipperfield, M. P., Carslaw, K. S., Sinnhuber, B.-M., Anderson, J. G., Stimpfle, R., Wilmouth, D., Fahey, D. W., Popp, P. J., Richard, E. C., von der Gathen, P., Jost, H., and Webster, C. R.: Modelling the effect of denitrification on Arctic ozone depletion during winter 1999/2000, J. Geophys. Res., 107, 8322, doi:10.1029/2001JD000445, 2002. 7647, 7648

Dobson, G. M. B.: Observer's handbook for the ozone spectrophotometer, Ann. Int. Geophys Year 5, 46–89, 1957. 7645

Eskes, H. J., van der A. R. J., Brinksma, E. J., Veefkind, J. P., de Haan, J. F., and Valks, P. J. M.: Retrieval and validation of ozone columns derived from measurements of SCIAMACHY

on Envisat, Atmos. Chem. Phys. Discuss., 5, 4429–4475, 2005, http://www.atmos-chem-phys-discuss.net/5/4429/2005/. 7646

Farman, J. C., Gardiner, B. G., and Shanklin, J. D.: Large losses of total ozone in Antarctica reveal seasonal ClO_x/NO_x interaction, Nature, 315, 207–210, 1985. 7642

Feng, W., Chipperfield, M. P., Davies, S., Sen, B., Toon, G., Blavier, J. F., Webster, C. R., Volk, C. M., Ulanovsky, A., Ravegnani, F., von der Gathen, P., Jost, H., Richard, E. C., and Claude, H.: Three-dimensional model study of the Arctic ozone loss in 2002/2003 and comparison with 1999/2000 and 2003/2004, Atmos. Chem. Phys., 5, 139–152, 2005, http://www.atmos-chem-phys.net/5/139/2005/. 7647

Feng W., M. P. Chipperfield, S. Davies, P. von der Gathen, E. Kyro, C. M. Volk, A. Ulanovsky and G. Belyaev: Large chemical ozone loss in 2004/05 Arctic winter/spring, Geophys. Res. Lett., 34, L09803, doi:10.1029/2006GL029098, 2007a. 7647

Feng, W., Chipperfield, M. P., Dorf, M., Pfeilsticker, K., and Ricaud, P.: Mid-latitude ozone changes: studies with a 3-D CTM forced by ERA-40 analyses, Atmos. Chem. Phys., 7, 2357–2369, 2007b, http://www.atmos-chem-phys.net/7/2357/2007/. 7647, 7648

Frieß, U., Kreher, K., Johnston, P. V., and Platt, U.: Ground-based DOAS measurements of stratospheric trace gases at two Antarctic stations during the 2002 ozone hole period, J. Atmos. Sci., 62, 765–777, 2005. 7644

Goutail, F., Pommereau, J.-P., Phillips, C.. Deniel, C., Sarkissian, A., Lefevre, F., Kyro, E., Rummukainen, M., Ericksen, P., Andersen, S., Kåstad Høiskar, B.-A., Braathen, G., Dorokhov, V., and Khattatov, V.: Depletion of column ozone in the Arctic during the Winters 1993-94 and 1994-95, J. Atmos. Chem., 32, 1–34, 1999. 7643, 7648

Goutail, F., Pommereau, J.-P., Lefèvre, F., van Roozendael, M., Andersen, S. B., Kåstad Høiskar, B.-A., Dorokhov, V., Kyrö, E., Chipperfield, M. P., and Feng, W.: Early unusual ozone loss during the Arctic winter 2002/2003 compared to other winters, Atmos. Chem. Phys., 5, 665–677, 2005, http://www.atmos-chem-phys.net/5/665/2005/. 7643, 7648

Hauchecorne, A., Godin, S., Marchand, M., Heese, B., and Souprayen, C.: Quantification of the transport of chemical constituents from the polar vortex to mid-latitudes in the lower stratosphere using the high-resolution advection model MIMOSA and effective diffusivity, J. Geophys. Res., 107(D20), 8289, doi:10.1029/2001JD000491, 2002. 7648

Lefèvre, F., Brasseur, G. P., Folkins, I., Smith, A. K., and Simon, P.: Chemistry of the 1991/1992

stratospheric winter: three dimensional model simulation, J. Geophys. Res., 99, 8183–8195, 1994. 7646

Lefèvre, F., Figarol, F., Carslaw, K. S., and Peter, T.: The 1997 Arctic ozone depletion quantified from three dimensional model simulations, Geophys. Res. Lett., 25, 2425–2428, 1998. 7646

Levelt, P. F., van den Oord, G. H. J., Dobber, M. R., Mlkki, A., Visser, H., de Vries, J., Stammes, P., Lundell, J., and Saari, H.: The Ozone Monitoring Instrument, IEEE T. Geosci. Remote Sens., 44, 1093–1101, 2006. 7645

Luo, B., Carslaw, K. S., Peter, T., and Clegg, S. L.: Vapour pressures of $H_2SO_4/HNO_3/HCl/HBr/H_2O$ solutions to low stratospheric temperatures, Geophys. Res. Lett., 22, 247–250, 1995. 7647

Nash, E. R., Newman, P. A., Rosenfield, J. E., and Schoeberl, M. R.: An objective determination of the polar vortex using Ertel's potential vorticity, J. Geophys. Res., 101, 9471–9478, 1996. 7648

Pommereau, J.-P. and Goutail, F.: Stratospheric O_3 and NO_2 Observations at the Southern Polar Circle in Summer and Fall 1988, Geophys. Res. Lett., 15, 891–894, 1988. 7644

Prather, M. J.: Numerical advection by conservation of second-order moments, J. Geophys. Res., 91, 6671–6681, 1986. 7648

Roscoe, H. K, Johnston, P. V., Van Roozendael, M., Richter, A., Preston, K., Lambert, J. C., Hermans, C., de Kuyper, W., Dzenius, S., Winterath, T., Burrows, J., Sarkissian, A., Goutail, F., Pommereau, J.-P., et al.: Slant column measurements of O_3 and NO_2 during the NDSC intercomparison of zenith-sky UV-visible spectrometers in June 1996, J. Atmos. Chem., 32, 281–314, 1999. 7644

Sander, S. P., Friedl, R. R., Golden, D. M., et al.: Chemical kinetics and photochemical data for use in atmospheric studies, Eval. 15, JPL Publ. 06-2, Jet Propul. Lab., Pasadena, USA, 2006. 7647, 7648

Vaughan, G., Roscoe, H. K, Bartlett, L. M., OĆonnor, F.M., Sarkissian, A., Van Roozendael, M., Lambert, J.-C., Simon, P. C., Karlsen, K., Kåstad Høiskar, B. A., Fish, D. J., Jones, R., Freshwater, L. R., Pommereau, J.-P., Goutail, F., Andersen, S. B., Drew, D. G., Hughes, P. A., Moore, D., Mellqvist, J., Hegels, E., Klupfel, T., Erle, F., Pfeilsticker, K., and Platt, U.: An intercomparison of ground-based UV visible sensors of Ozone and NO_2, J. Geophys. Res., 102, 1411–1422, 1997. 7644

Williamson, D. L. and Rasch, P. J.: Two-dimensional semi-Lagrangian transport with shape-preserving interpolation, Mon. Weather Rev., 117, 102–129, 1989. 7647

WMO (World Meteorological Organization): The Global Atmosphere Watch Guide, WMO TD No. 553, 1993. 7643

WMO (World Meteorological Organization): Scientific assessment of ozone depletion: 2006, Global Ozone Research and Monitoring Project-Report No. 50, 572 pp., Geneva, Switzerland, 2007. 7647

Table 1. Measurement sites, latitude (Lat.), longitude (Long.), type of observation (Inst.) and starting period of observation (St. yr.), for which the ozone loss analyses were performed.

Station	Lat.	Long.	Inst.	St. yr.
Amundsen-Scott	89.9° S	24.8° W	Dobson	1963
Belgrano	77.9° S	34.6° W	Brewer	1982
Arrival Heights	77.8° S	166.7° W	Dobson	1988
Halley	75.6° S	26.8° W	Dobson	1958
Concordia	75.1° S	123.4° E	SAOZ	2007
Neumayer	70.7° S	8.3° W	DOAS	1992
Zhongshan	69.4° S	76.4° E	Brewer	1993
Syowa	69.0° S	39.6° E	Dobson	1961
Rothera	67.6° S	68.1° W	SAOZ	1996
Dumont d'Urville	66.7° S	140.0° E	SAOZ	1988
Faraday/Vernadsky	65.3° S	64.3° W	Dobson	1957
Marambio	64.2° S	56.7° W	Dobson	1987
Mid-Lat. stations				
Ushuaia	54.8° S	68.2° W	Dobson	1994
Macquarie Isl.	54.5° S	159° E	Dobson	1957
Rio Gallegos	51.6° S	69.3° W	SAOZ	2008
Kerguelen	49.4° S	70.3° E	SAOZ	1995
Lauder	45.0° S	169.6° E	Dobson	1970

Table 2. Vortex averaged ozone loss estimated using ground-based (GB), OMI and Sciamachy (SCIA) observations and the total column integrated from Reprobus (2006–2009) and SLIMCAT (2005) simulations (MODEL), during the recent Antarctic winters. Extrapolated data are used for day 225 to calculate the ozone loss rates in 2007 and 2009 from SCIA.

Year	Data	Max. loss		Loss rate (/day)	
		DU	%	DU	%
2009	GB	205	53	2.41	0.62
	OMI	240	53	2.28	0.58
	SCIA	217	51	2.16	0.54
	MODEL	210	54	2.22	0.55
2008	GB	227	59	3.22	0.84
	OMI	240	60	3.37	0.88
	SCIA	237	57	2.52	0.68
	MODEL	238	60	3.00	0.77
2007	GB	228	55	2.45	0.62
	OMI	232	55	2.35	0.54
	SCIA	222	52	1.76	0.47
	MODEL	228	58	2.60	0.66
2006	GB	179	56	2.25	0.71
	OMI	177	55	2.08	0.65
	SCIA	176	53	1.85	0.58
	MODEL	174	53	2.26	0.71
2005	GB	245	61	2.23	0.53
	OMI	234	58	2.12	0.50
	SCIA	244	60	1.72	0.50
	MODEL	249	63	3.06	0.75

Fig. 1. The SAOZ instrument at Dumont d'Urville in the Antarctic.

ACPD

10, 7641–7674, 2010

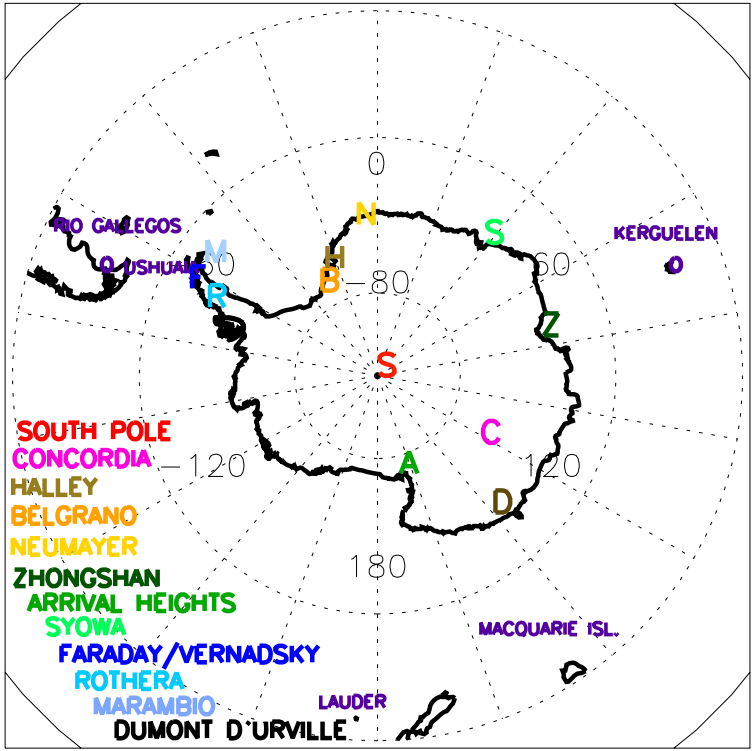

Fig. 2. The ground-based stations in the Antarctic and mid-latitudes that are used in the ozone loss analyses.

ACPD
10, 7641–7674, 2010

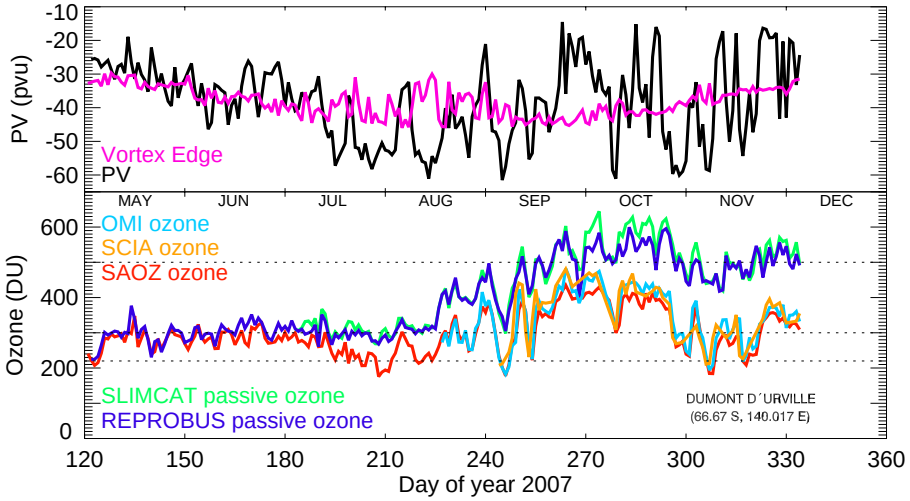

Fig. 3. Bottom: daily mean SAOZ total ozone at Dumont d'Urville in winter-spring 2007 compared to OMI and Sciamachy (SCIA) overpasses and the integrated passive ozone column from the models. Top: the ECMWF potential vorticity at 475 K above the station and the polar vortex edge. Shown by horizontal bars are the 220 DU ozone hole definition value, the 300 DU average pre-ozone hole value and the 500 DU average spring column in the absence of depletion.

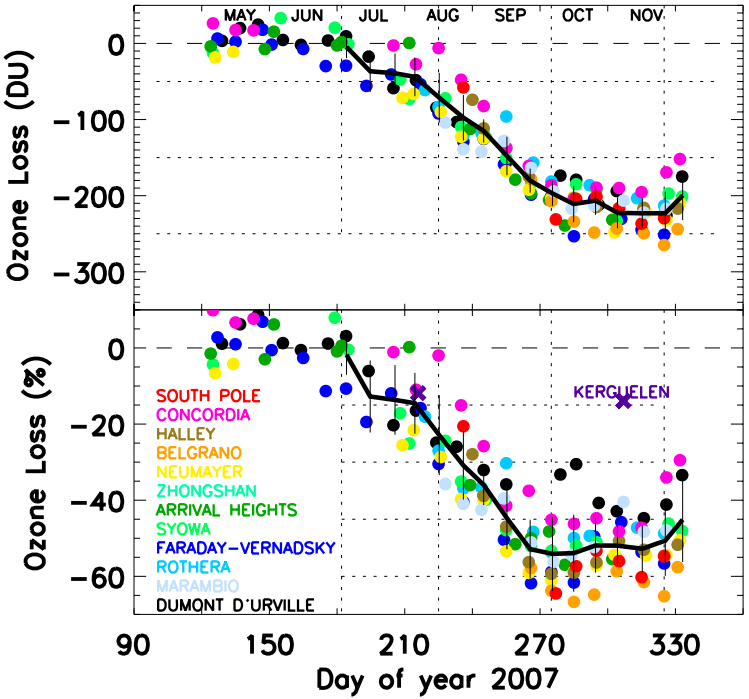

Fig. 4. Vortex averaged (ten-day mean) individual ozone loss estimated at the ground-based sites in the Antarctic using the passive method (top: DU, bottom: percent). The black solid lines represent the mean and the vertical bars represent standard deviations. The observations from Kerguelen, a mid-latitude station, are not included in the average, shown with "x" marks. The vertical dotted lines represent days 182, 225, 275 and 325, while the horizontal lines represent 50, 150 and 250 DU and 15, 30, 45 and 60% of ozone loss.

ACPD
10, 7641–7674, 2010

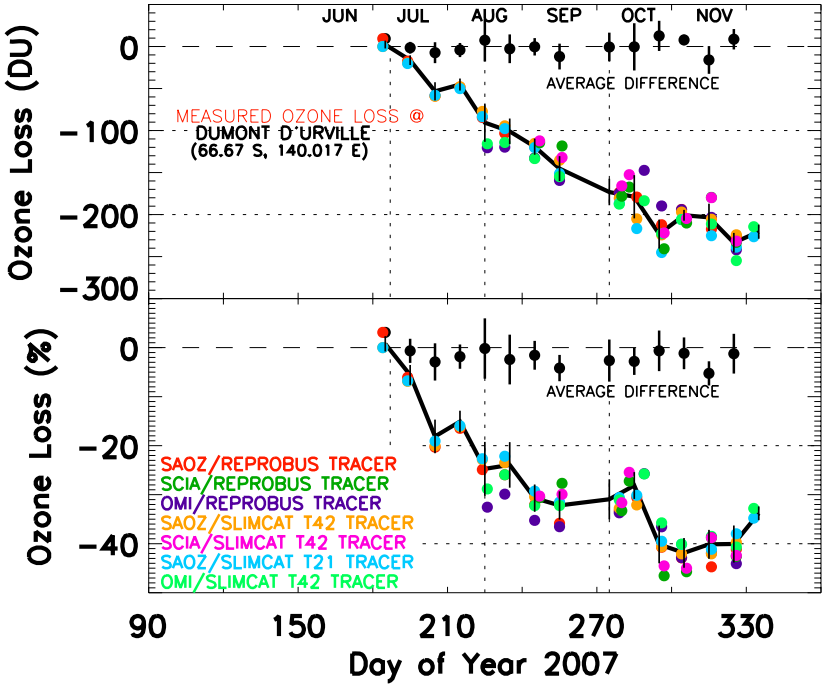

Fig. 5. Vortex averaged (ten-day mean) ozone loss diagnosed using different measurements and model setups. The black solid lines represent the mean ozone loss from all scenarios and the black filled-circles represent the average deviation from the control (SAOZ/REPROBUS tracer). The vertical bars represent the standard deviation from the mean. The dotted vertical lines represent days 182, 225 and 275 and the dotted horizontal lines represent 100 and 200 DU and 20 and 40% of ozone loss.

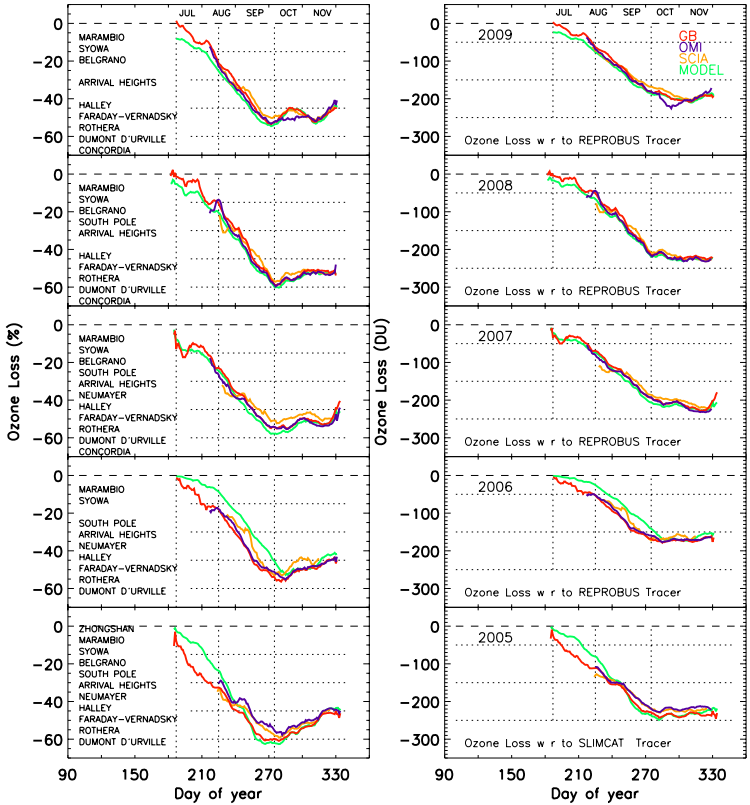

Fig. 6. Vortex averaged (five-day running mean) ozone loss estimated from the ground-based (GB) measurements in red, as listed in the figure, the OMI observations in blue (OMI), the Sciamachy measurements in dark yellow (SCIA) and the model simulations by REPROBUS in 2006–2009 and SLIMCAT in 2005 in green (MODEL) for the Antarctic winters 2005–2009. The SCIA average excludes South Pole measurements due to unavailability. The dotted vertical lines represent days 187, 225 and 275. Left: percent, right: DU.

ACPD
10, 7641–7674, 2010

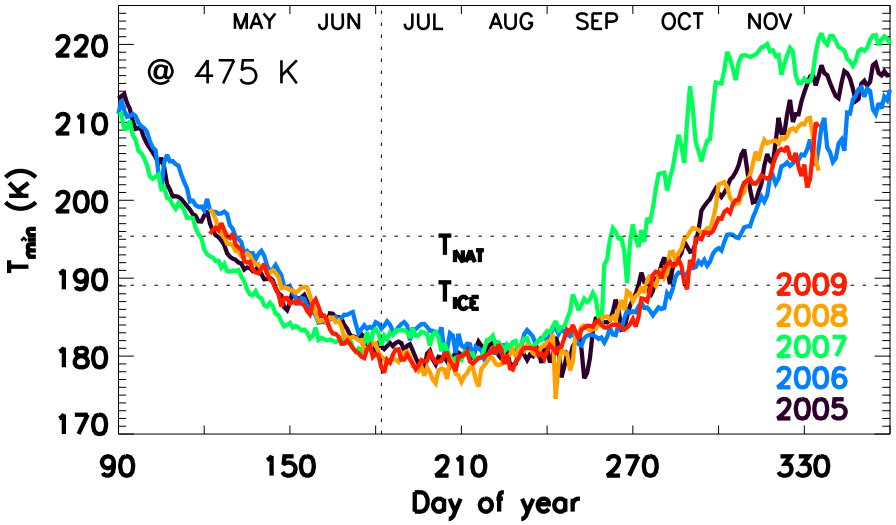

Fig. 7. ECMWF daily minimum temperatures within 50–90° S at 475 K for 2005–2009. The horizontal lines represent the T_{NAT} and T_{ICE} thresholds. The dotted vertical line shows day 182.

ACPD
10, 7641–7674, 2010

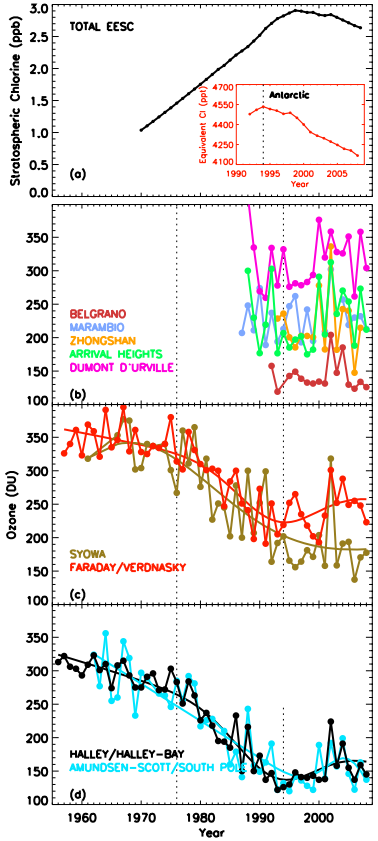

Fig. 8. October monthly mean total ozone from the Antarctic stations and **(a)** total stratospheric chlorine and the equivalent chlorine in the inset. **(b)** Stations installed after 1985, **(c)** historical stations in the West Antarctic and **(d)** historical stations in the Central Antarctic. The dotted vertical lines represent years 1976 and 1994. A Gaussian fit is shown in the time series of the historical stations.

ACPD
10, 7641–7674, 2010

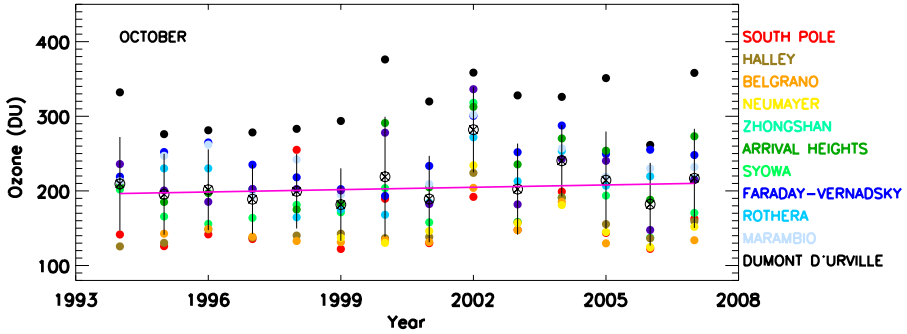

Fig. 9. October monthly mean total ozone at the Antarctic stations for 1994–2007. The mean ozone from all the stations is shown by "x" signs and the magenta line represents a simple linear regression.

ACPD
10, 7641–7674, 2010

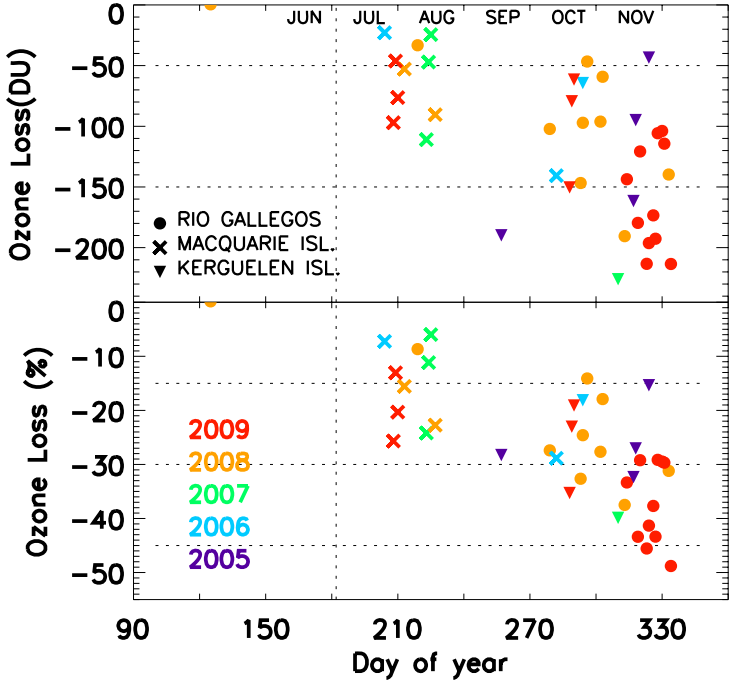

Fig. 10. Vortex averaged ozone loss estimated (using Reprobus tracer) at selected southern mid-latitude stations for recent winters. The dotted vertical line represents day 182 and the horizontal lines show 50 and 150 DU and 15, 30 and 45% of ozone loss. Top: DU, bottom: percent.

ACPD
10, 7641–7674, 2010

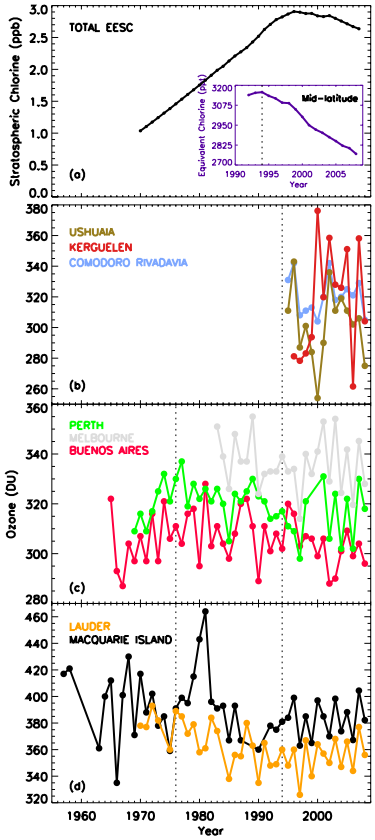

Fig. 11. Time series of October monthly mean total ozone from selected mid-latitude Dobson stations and **(a)** total stratospheric chlorine together with equivalent chlorine in the mid-latitudes in the inset, **(b)** stations installed since 1985, **(c)** historical stations at 30–40° S, and **(d)** historical stations at 40–60° S. The dotted vertical lines represent years 1976 and 1994.